Coherent Beam Splitting of Flying Electrons Driven by a Surface Acoustic Wave

R. Ito,[1,*] S. Takada,[2] A. Ludwig,[3] A. D. Wieck,[3] S. Tarucha,[1] and M. Yamamoto[1,†]
[1]Center for Emergent Matter Science, RIKEN, 2-1 Hirosawa, Wako, Saitama 351-0198, Japan
[2]National Institute of Advanced Industrial Science and Technology, National Metrology Institute of Japan, 1-1-1 Umezono, Tsukuba, Ibaraki 305-8563, Japan
[3]Angewandte Festkörperphysk, Ruhr-Universität Bochum, D-44780 Bochum, Germany

(Received 23 April 2020; accepted 7 January 2021; published 16 February 2021)

We develop a coherent beam splitter for single electrons driven through two tunnel-coupled quantum wires by surface acoustic waves (SAWs). The output current through each wire oscillates with gate voltages to tune the tunnel coupling and potential difference between the wires. This oscillation is assigned to coherent electron tunneling motion that can be used to encode a flying qubit and is well reproduced by numerical calculations of time evolution of the SAW-driven single electrons. The oscillation visibility is currently limited to about 3%, but robust against decoherence, indicating that the SAW electron can serve as a novel platform for a solid-state flying qubit.

DOI: 10.1103/PhysRevLett.126.070501

In quantum optics, quantum information is encoded on photons, called flying qubits. A new approach for quantum computation has recently been proposed in which a qubit array can be stored in a loop of an optical channel and universal operations can be achieved by connecting only a few fundamental physical gates to the optical channel [1,2]. Such an architecture of the photon flying qubits is different from those of solid-sate qubits that require the physical gate structures to be scalable. Similarly, quantum circuits of electrons propagating through one-dimensional (1D) wires are also able to host electrons as flying qubits. In previous studies, single flying qubit manipulation has been demonstrated in electronic Mach-Zehnder interferometers [3,4]. However, the flying qubits in these studies consist of electrons continuously injected from the static macroscopic reservoirs, and therefore, the electron wave functions are spatially spread along the longitudinal direction. Thus, these qubits are incompatible with the photon qubit arrays in quantum optics.

On the other hand, various on-demand sources of finite-size single electrons that resemble the photon arrays have recently been demonstrated [5–13]. One of the ways is to use a surface acoustic wave (SAW) and a depleted 1D channel made in a piezoelectric medium. The SAW generates a moving electrostatic potential [moving quantum dot (MQD)] to capture a single electron from a reservoir or a static quantum dot and transports it, while confining it in the SAW potential minimum [14–16]. The SAW-driven electron transport allows us to create a qubit array, encoded on a train of single electrons, whose spacing is much smaller than the optical qubit spacing. Therefore, the SAW-driven electrons can be a promising candidate to construct a scalable quantum computing system, resembling the photon arrays.

Among the required functions for SAW-driven flying-electron-based quantum computing, efficient on-demand single electron emission and detection have already been achieved [12]. The spin information of the SAW-driven single electron is also preserved while being transferred between distant quantum dots through a depleted 1D channel [11]. Manipulation of its spin using the spin-orbit interaction during transportation has also been demonstrated [17]. One of the remaining challenges to implement the flying electron qubits is the quantum manipulation of the orbital state of a SAW-driven single electron. A fully tunable coherent beam splitter is a key ingredient in the flying qubit operation; however, its demonstration has still been elusive owing to technical difficulties.

The coherent beam splitter for SAW-driven single electrons was proposed more than a decade ago [18]. It consists of two tunnel-coupled parallel quantum wires [19–21], and the qubit state is encoded by electron occupation of either of the tunnel-coupled wires (TCWs). Although there are some reports demonstrating splitting or directional control of the electron flow in a similar device [12,18,22–24], coherent tunneling of SAW-driven electrons propagating through the TCWs has never been addressed so far.

Here, we realize the coherent beam splitting of SAW-driven single electrons in the TCWs. The SAW potential loads single electrons from a reservoir to its potential minima to construct an array of single electrons that are transported with a fixed time interval. We measure two output currents obtained for the SAW-driven electrons passing the TCWs and find them consistent with numerical calculations. The visibility of the coherent beam splitting we obtained is low, but robust against increase in temperature. To the best of our knowledge, this is the first

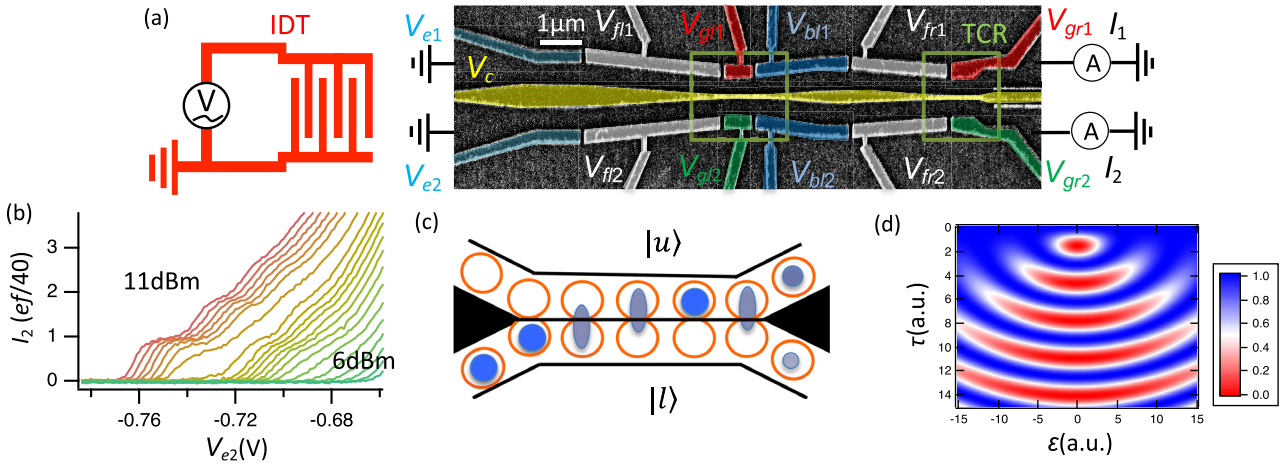

FIG. 1. (a) Scanning electron microscope image of TCWs. Two TCRs are indicated by the green square flames. An IDT is placed 1.3 mm away from the TCWs to the left. (b) Quantized current, observed when SAW-driven single electrons are injected to the left bottom wire, as a function of V_{e2} with keeping V_c constant at -1 V. The microwave power applied on the IDT is varied from 11 (red) to 6 dBm (green) in steps of 0.25 dBm. (c) Schematic of the TCR with propagation of SAW-driven single electrons. (d) Calculation of electron tunnel oscillation pattern (output current of the lower channel normalized by the total current) as a function of the tunneling energy (τ) and detuning (ϵ) using a two-site Hubbard model.

demonstration of a coherent electron beam splitter, which serves as a milestone toward the realization of on-demand single electron quantum optical devices.

The device used in our experiment is made out of GaAs/AlGaAs heterostructure, which contains a two-dimensional electron gas with a mobility of 1.5×10^6 cm^2/Vs and carrier density of 1.46×10^{11} cm^{-2}. Two TCWs are defined by using a Schottky gate technique and they are only tunnel coupled in two separate tunnel-coupled regions (TCRs) [see two square frames in Fig. 1(a)]. Both wires are depleted to isolate the SAW-driven electrons from the electrons in the surrounding area. An interdigital transducer (IDT) that converts microwaves to SAWs is placed 1.3 mm away from the entrance of the 1D wires. The period of the IDT fingers, i.e., the SAW wavelength is 1 μm, while the number of the IDT periods is 100. A 13-dBm microwave is applied to the IDT with 1/40 duty cycle to avoid heating of the entire device [25,26].

The SAW-driven electronic current through the wire is quantized at nef times the duty cycle of 1/40, where n is the number of electrons in each MQD, e is the elementary charge, and f is the SAW frequency [Fig. 1(b)]. We use the first quantized SAW current as an electron source, where the number of electrons loaded in each MQD is one. The electrons are transported through the lower wire to one of the TCRs at the SAW velocity of 2.7 km/s. Gate voltages applied to deplete the lower wire are adjusted such that the potential slope along the wires is slightly upward in the transport direction until electrons reach the TCR, thus protecting the electron from dropping forward the MQD.

In the TCR, MQDs from the upper and lower wires are coupled and the trapped electron becomes able to tunnel into the other MQD, as shown in Fig. 1(c) (see Supplemental Material [27] for details). We use the two-site Hubbard model to describe the electron state (flying qubit) evolution in the TCR. The Hamiltonian is given by

$$H = \frac{\epsilon}{2}|l\rangle\langle l| - \tau|u\rangle\langle l| - \tau|l\rangle\langle u| - \frac{\epsilon}{2}|u\rangle\langle u|, \qquad (1)$$

where τ is the interchannel tunnel-coupling energy and ϵ is the detuning defined as the on site energy difference between the two MQDs. The flying qubit state is encoded based on whether the electron trapped by the MQD is in the upper ($|u\rangle$) or lower ($|l\rangle$) MQD. The time evolution of the electron state is represented as $|\phi(t)\rangle = e^{(-iHt/\hbar)}|\phi(0)\rangle$ with $|\phi(0)\rangle = |l\rangle$. The electron periodically oscillates between the two MQDs by tunneling through the center barrier during the transportation. The probability of an electron flowing out of the lower wire measured as the output current is calculated as a function of ϵ and τ and is shown in Fig. 1(d).

In our experiment, coherent interwire tunneling of SAW-driven electrons is investigated by sweeping the side gate voltages V_{gr1} and V_{gr2} (V_{gl1} and V_{gl2}) for the right (left) TCR [see Fig. 1(a)]. These voltages can be used to simultaneously tune both τ and ϵ for a fixed center-gate voltage V_c. The difference between the side gate voltages, $V_{gdr} = V_{gr1} - V_{gr2}$ ($V_{gdl} = V_{gl1} - V_{gl2}$) is a control parameter for ϵ, while their average, $V_{gsr} = (V_{gr1} + V_{gr2}/2)$ ($V_{gsl} = (V_{gl1} + V_{gl2}/2)$), to modify the coupling energy τ for the right (left) TCR. Even though there are two TCRs in the device, only one of them is adjusted to have an appropriate tunnel coupling in the experiment. The other is tuned to have two wires isolated.

Figure 2(a) shows the current I_2 measured at the output contact of the lower channel of the right TCR as a function

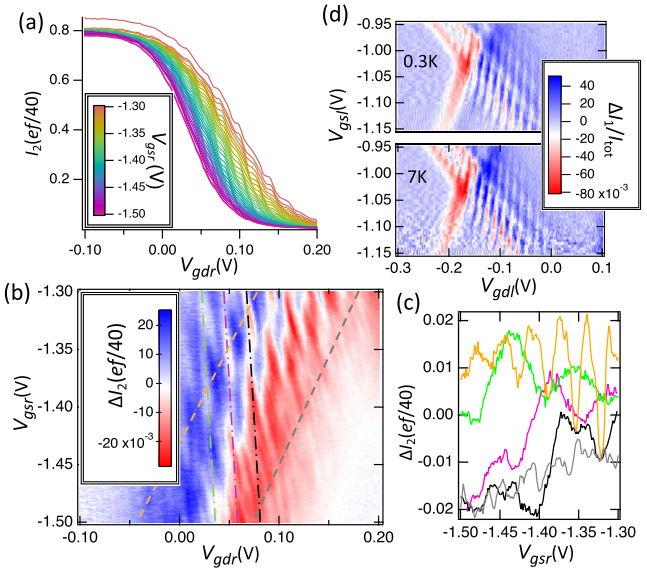

FIG. 2. (a) Output current I_2 measured at the lower Ohmic contact as a function of $V_{gdr} = V_{gr1} - V_{gr2}$. Electrons are injected from the lower wire and the right TCR in Fig. 1(a) is used. $V_c = -0.7$ V and $V_{fr1} = V_{fr2} = -1.3$ V. (b) The oscillating component ΔI_2 of the current obtained by subtracting the smoothed background from the raw data in (a). (c) ΔI_2 along the dashed lines and dot-dashed lines in (b) plotted as functions of V_{gsr}. The colors correspond with those in (b). (d) ΔI_1 normalized by the total current ($I_{\rm tot}$) measured at 0.3 and 7 K. The left TCR is used. Since electrons are injected from the upper wire, the structure of ΔI_1 is inverted along V_{sdl} from that of (b). The gate voltages are $V_c = -0.7$ V, $V_{fl1} = V_{fl2} = -1.2$ V, and $V_{bl1} = V_{bl2} = -1.3$ V, respectively.

of V_{gdr} and V_{gsr}. The current I_1 at the other output varies simultaneously such that the total current $I_{\rm tot} = I_1 + I_2$ is constant (I_1 and $I_{\rm tot}$ are not shown). $I_{\rm tot}$ is approximately $0.8ef/40$, less than the quantized value ef times the duty cycle, although it was tuned by V_{e2} at the first quantized plateau. This is probably because there is a finite probability of an electron escaping from the MQD and being backscattered while traveling through the long entire depleted 1D wires. For $V_{gdr} < -0.05$ V, $I_2 = I_{\rm tot}$, indicating that all electrons flow through the lower wire. As V_{gdr} is made more positive, I_2 becomes smaller with accompanying ripples and finally quenched for $V_{gdr} > 0.2$ V, indicating that all electrons flow through the upper wire. Note that the ripple structure is suppressed when the number of electrons in each MQD is increased over one (see Supplemental Material [27]). To highlight the ripple structure, we subtract the background derived by smoothing the raw data along V_{gdr} and plot the outcome (ΔI_2) as a function of V_{gdr} and V_{gsr} in Fig. 2(b) (see Supplemental Material [27] for I_2). Though the oscillation pattern does not resemble that derived from the simple two-level model [Fig. 1(d)], we find that an enlarged view of the pattern in Fig. 2 shows a similarity as explained below.

In Fig. 2(b) we observe current oscillations in two directions as indicated by the dot-dashed and dashed lines, respectively. We here take the higher-lying orbital states in each MQD into account to explain these oscillations based on knowledge from the numerical simulation (explained later). Along the dot-dashed lines, one of the higher-lying orbital states in the upper MQD and the initially loaded state in the lower MQD are energetically aligned. The tunnel-coupling energy τ between the MQD states changes with V_{gsr}, causing the current oscillation. Since τ gradually changes with V_{gsr} compared to ϵ with V_{gdr}, the WiFi-symbol-like pattern in Fig. 1(d) is squeezed horizontally to become like the oscillation along the dot-dashed line. On the other hand, along the dashed line, different higher-lying orbital states in the upper MQD are sequentially aligned with the initially loaded state in the lower MQD. The tunnel-coupling energy between the MQD states is tuned to be constant along the dashed lines, and thus I_2 becomes small every time the MQD states align, providing current oscillation. Figure 2(c) shows ΔI_2 along the dot-dashed and dashed lines in Fig. 2(b). The maximum visibility of the current oscillation obtained is about 3% for the dashed line in yellow and 2% for the dot-dashed line in green, respectively.

To support the above description and study inherent problems for realizing a coherent beam splitter, we numerically simulate the electron motion in a TCR. The potential profile is calculated for the gate geometry similar to that of the left TCR in Fig. 1(a) by solving Laplace's equation using a finite element method [see Figs. 4(d)–4(f) and the Supplemental Material [27]]. The electron motion is then numerically calculated by solving the time-dependent Schrödinger equation [28]. We assume that the amplitude of the SAW-induced moving potential is 20 mV, as obtained experimentally using the method described by Fletcher *et al.* [29], and that this value is not affected by the surface gates [30–32]. The initial electron state is assumed to be in the ground state confined in the MQD in the lower wire.

The calculated probability $P_{\rm out}$ of the SAW-driven electron, staying in the lower 1D wire, is shown in Fig. 3. $P_{\rm out}$ reproduces well the experimentally observed features, i.e., two families of current oscillations along the dot-dashed and dashed lines in Fig. 2(b). We figure out the origin of the two current oscillation families by analyzing the time evolution of a SAW-driven electron.

Figure 4 shows the calculated time evolution of the electron state at each gate voltage marked by the green circle, square and triangle in Fig. 3, respectively. Figures 4(a)–4(c) show the probability P_l (P_u) of finding the electron in the lower (upper) wire by the green (red) line. On the other hand, Figs. 4(d)–4(f) show the accumulation of 24 datasets of the spatial probability distribution (SPD) at fixed time intervals of 15.4 ps. Over the 24 datasets, the SAW travels by 1 μm. These plots show the trajectory of electrons and shapes of the wave function in

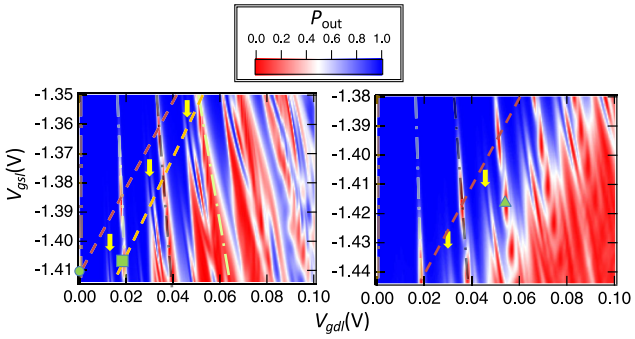

FIG. 3. Numerically calculated probability P_{out} of electron staying in the lower wire through the TCR. Left: typical result when electrons are fully trapped by the SAW potential during the time evolution. $V_c = -1$ V, $V_{fl1} = V_{fl2} = -1.1$ V, $V_{bl1} = V_{bl2} = -1.2$ V. Right: typical result when a party of electrons drop off the SAW potential at the middle of the TCR. $V_c = -1$ V, $V_{fl1} = V_{fl2} = -1.1$ V, $V_{bl1} = V_{bl2} = -1$ V.

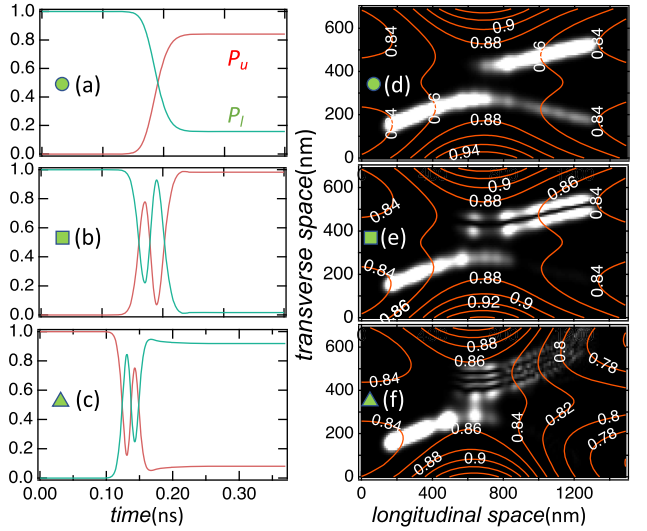

FIG. 4. Calculated temporal and spatial distribution of an electron in the TCW for each marked point in Fig. 3. (a)–(c) Probability of finding an electron in the lower channel, P_l in green and upper channel, P_u in red, respectively, at each time instance. (d)–(f) Cumulative SPDs of those obtained at the time intervals of 15.4 ps with contour plots of the potential profile.

the transverse direction, and therefore profile the orbital states that contribute to the interwire tunneling of the electrons. For example, the green square is placed on the crossing of the second leftmost dot-dashed line and second topmost dashed line in the left panel of Fig. 3. At this point, the ground state of the lower MQD, having no node in SPD, and the first excited state of the upper MQD, having one node along the transverse direction, are in resonance [see Fig. 4(e)]. Note that the electron is in the ground state in each MQD along the longitudinal direction. Resonance of the ground and first excited state is maintained on the second leftmost dot-dashed line, changing the frequency of tunnel oscillation, i.e., number of electron tunneling. At the green square point, the SAW-driven electron undergoes three times tunneling between the wires as shown in Fig. 4(b). The oscillation number is fixed on the second topmost dashed line. The same rule applies to the lines running through the green circle: The ground state is aligned between the upper and lower MQD and the electron tunnels only once from the lower to upper MQD as shown in Fig. 4(a).

Finally, we address the case where V_{bl1} and V_{bl2} are set to be more positive (right panel of Fig. 3). In this situation, electrons drop off the MQD forward at the end of the TCR. The time evolution of P_l, P_u, and SPD at the triangle mark are plotted at Figs. 4(c) and 4(f). In Fig. 4(f), SPD is suppressed at $x > 800$ nm because the electron quickly escapes from the MQD. This results in a more distinct current oscillation along the dot-dashed line in Fig. 3 (right), because a superposition state at the end of the TCR does not adiabatically fall into a local state ($|u\rangle$ or $|l\rangle$) in one of the two wires. We cannot determine whether an electron is trapped in or dropped from the MQD in the experiment with the right TCR [Fig. 2(b)]. However, with the left TCR we observe that the tunneling signal becomes clearer by increasing V_{bl1} and V_{bl2} (see Supplemental Material [27]).

The visibility of current oscillation along the dashed line in Fig. 3 is almost unity in the numerical calculation. It suggests it is possible to generate tunnel oscillation with high visibility, whereas the current oscillation visibility actually observed is pretty low (3%). We studied a dephasing problem as a possible origin for the low visibility. Figure 2(d) shows comparison of the tunneling oscillation measured at 0.3 and 7 K. There is no distinguishable change in the oscillation visibility with temperature. We note that 7 K is the limit of measurable temperature in our setup. The dominant dephasing source for the electron orbital state is usually not the charge noise because it is weak [33], but coupling to phonons as demonstrated for static double quantum dots [34]. However, the phonon dephasing should depend on temperature, and therefore, it seems negligible. This is probably because of the short dwell time of $\lesssim 300$ ps during which the electron propagates through the TCR and consistent with the theoretical calculation for charge qubits in a static double quantum dot [35].

Then, what is the origin for the low visibility? This may be assigned to poor fidelity of initialization of the electron wave function in the MQD entering the TCR. Electrons can be loaded directly to the excited states from the reservoirs. The potential roughness induced by dopants in a depleted quantum wire can also scatter the electrons into excited states. Typically, excited states have higher tunnel-coupling energies than the ground state for the identical gate configuration. Thus, the raw tunneling current constituted from multiple excited states monotonically changes along the dot-dashed line in Fig. 2(b)

(see Supplemental Material [27]) and the inter-MQD tunneling signal is blurred. A device fabricated on a wafer having less impurities such as undoped GaAs may improve the visibility [36,37].

In the numerical calculations, small dips of P_{out} are observed as indicated by yellow arrows (Fig. 3), although not visible in Fig. 2(b). These dips originate from the tunnel coupling between the initially loaded ground state in the lower MQD and the higher excited states confined by the SAW potential along the traveling direction in the upper MQD. The tunnel coupling between these states is weak, because the corresponding wave functions are almost orthogonal to each other; thus, these minor dips only appear for more negative V_{gs}, where the tunnel coupling is larger.

In summary, we observe coherent tunneling of SAW-driven single electrons between the two depleted, but tunnel-coupled 1D wires. The coherent tunneling occurs when the MQDs are energetically aligned between the two wires with interchannel tunneling strength and energy detuning as control parameters. The experimental data compare well to the numerical calculation. This study is an important step toward realization of solid-state flying qubits.

We acknowledge fruitful discussion with Christopher Bäuerle. M. Y. acknowledges support from KAKENHI (Grant No. 18H04284) and CREST-JST (No. JPMJ CR1876). Se. T. acknowledges support from CREST-JST (No. JPMJCR1675) and KAKENHI (Grant No. 26220 710). A. L. and A. D. W. acknowledge gratefully support of DFG-TRR160, BMBF—Q.Link.X 16KIS0867, and the DFH/UFA CDFA-05-06. Sh. T. acknowledges support from KAKENHI (Grant No. 20H02559). The numerical calculations in this study were performed using the Fujitsu PRIMERGY CX600M1/CX1640M1 (Oakforest-PACS) in the Information Technology Center, The University of Tokyo.

*ryo.ito@riken.jp
†michihisa.yamamoto@riken.jp

[1] S. Takeda and A. Furusawa, Universal Quantum Computing with Measurement-Induced Continuous-Variable Gate Sequence in a Loop-Based Architecture, Phys. Rev. Lett. **119**, 120504 (2017).

[2] S. Takeda, K. Takase, and A. Furusawa, On-demand photonic entanglement synthesizer, Sci. Adv. **5**, eaaw4530 (2019).

[3] Y. Ji, Y. Chung, D. Sprinzak, M. Heiblum, D. Mahalu, and H. Shtrikman, An electronic Mach-Zehnder interferometer, Nature (London) **422**, 415 (2003).

[4] M. Yamamoto, S. Takada, C. Bäuerle, K. Watanabe, A. D. Wieck, and S. Tarucha, Electrical control of a solid-state flying qubit, Nat. Nanotechnol. **7**, 247 (2012).

[5] G. Fève, A. Mahé, J. M. Berroir, T. Kontos, B. Plaçais, D. C. Glattli, A. Cavanna, B. Etienne, and Y. Jin, An on-demand coherent single-electron source, Science **316**, 1169 (2007).

[6] J. Dubois, T. Jullien, F. Portier, P. Roche, A. Cavanna, Y. Jin, W. Wegscheider, P. Roulleau, and D. C. Glattli, Minimal-excitation states for electron quantum optics using levitons, Nature (London) **502**, 659 (2013).

[7] T. Jullien, P. Roulleau, B. Roche, A. Cavanna, Y. Jin, and D. C. Glattli, Quantum tomography of an electron, Nature (London) **514**, 603 (2014).

[8] R. Bisognin, A. Marguerite, B. Roussel, M. Kumar, C. Cabart, C. Chapdelaine, A. Mohammad-Djafari, J. M. Berroir, E. Bocquillon, B. Plaçais, A. Cavanna, U. Gennser, Y. Jin, P. Degiovanni, and G. Fève, Quantum tomography of electrical currents, Nat. Commun. **10**, 3379 (2019).

[9] R. P. G. McNeil, M. Kataoka, C. J. B. Ford, C. H. W. Barnes, D. Anderson, G. A. C. Jones, I. Farrer, and D. A. Ritchie, On-demand single-electron transfer between distant quantum dots, Nature (London) **477**, 439 (2011).

[10] S. Hermelin, S. Takada, M. Yamamoto, S. Tarucha, A. D. Wieck, L. Saminadayar, C. Bäuerle, and T. Meunier, Electrons surfing on a sound wave as a platform for quantum optics with flying electrons, Nature (London) **477**, 435 (2011).

[11] B. Bertrand, S. Hermelin, S. Takada, M. Yamamoto, S. Tarucha, A. Ludwig, A. D. Wieck, C. Bäuerle, and T. Meunier, Fast spin information transfer between distant quantum dots using individual electrons, Nat. Nanotechnol. **11**, 672 (2016).

[12] S. Takada, H. Edlbauer, H. V. Lepage, J. Wang, P.-A. Mortemousque, G. Georgiou, C. H. W. Barnes, C. J. B. Ford, M. Yuan, P. V. Santos, X. Waintal, A. Ludwig, A. D. Wieck, M. Urdampilleta, T. Meunier, and C. Bäuerle, Sound-driven single-electron transfer in a circuit of coupled quantum rails, Nat. Commun. **10**, 4557 (2019).

[13] C. Bäuerle, D. C. Glattli, T. Meunier, F. Portier, P. Roche, P. Roulleau, S. Takada, and X. Waintal, Coherent control of single electrons: A review of current progress, Rep. Prog. Phys. **81**, 056503 (2018).

[14] J. M. Shilton, V. I. Talyanskii, M. Pepper, D. A. Ritchie, J. E. F. Frost, C. J. B. Ford, C. G. Smith, and G. A. C. Jones, High-frequency single-electron transport in a quasi-one-dimensional GaAs channel induced by surface acoustic waves, J. Phys. Condens. Matter **8**, L531 (1996).

[15] V. I. Talyanskii, J. M. Shilton, M. Pepper, C. G. Smith, C. J. B. Ford, E. H. Linfield, D. A. Ritchie, and G. A. C. Jones, Single-electron transport in a one-dimensional channel by high-frequency surface acoustic waves, Phys. Rev. B **56**, 15180 (1997).

[16] C. H. W. Barnes, J. M. Shilton, and A. M. Robinson, Quantum computation using electrons trapped by surface acoustic waves, Phys. Rev. B **62**, 8410 (2000).

[17] H. Sanada, Y. Kunihashi, H. Gotoh, K. Onomitsu, M. Kohda, J. Nitta, P. V. Santos, and T. Sogawa, Manipulation of mobile spin coherence using magnetic-field-free electron spin resonance, Nat. Phys. **9**, 280 (2013).

[18] M. Kataoka, C. H. W. Barnes, C. J. B. Ford, H. E. Beere, D. A. Ritchie, D. Anderson, G. A. C. Jones, and M. Pepper, Single-electron transfer between double quantum dots defined by surface acoustic waves, Physica (Amsterdam) **34E**, 546 (2006).

[19] J. A. del Alamo and C. C. Eugster, Quantum field-effect directional coupler, Appl. Phys. Lett. **56**, 78 (1990).
[20] N. Tsukada, A. D. Wieck, and K. Ploog, Proposal of novel electron wave coupled devices, Appl. Phys. Lett. **56**, 2527 (1990).
[21] A. Bertoni, P. Bordone, R. Brunetti, C. Jacoboni, and S. Reggiani, Quantum Logic Gates Based on Coherent Electron Transport in Quantum Wires, Phys. Rev. Lett. **84**, 5912 (2000).
[22] V. I. Talyanskii, M. R. Graham, and H. E. Beere, Acousto-electric y-branch switch, Appl. Phys. Lett. **88**, 083501 (2006).
[23] M. Kataoka, M. R. Astley, A. L. Thorn, C. H. W. Barnes, C. J. B. Ford, D. Anderson, G. A. C. Jones, I. Farrer, D. A. Ritchie, and M. Pepper, Investigation of single-electron dynamics in tunnelling between zero- and one-dimensional states, Physica (Amsterdam) **40E**, 1017 (2008).
[24] M. Kataoka, M. R. Astley, A. L. Thorn, D. K. L. Oi, C. H. W. Barnes, C. J. B. Ford, D. Anderson, G. A. C. Jones, I. Farrer, D. A. Ritchie, and M. Pepper, Coherent Time Evolution of a Single-Electron Wave Function, Phys. Rev. Lett. **102**, 156801 (2009).
[25] P. Utko, P. E. Lindelof, and K. Gloos, Heating in single-electron pumps driven by surface acoustic waves, Appl. Phys. Lett. **88**, 202113 (2006).
[26] R. J. Schneble, M. Kataoka, C. J. B. Ford, C. H. W. Barnes, D. Anderson, G. A. C. Jones, I. Farrer, D. A. Ritchie, and M. Pepper, Quantum-dot thermometry of electron heating by surface acoustic waves, Appl. Phys. Lett. **89**, 122104 (2006).
[27] See Supplemental Material at http://link.aps.org/supplemental/10.1103/PhysRevLett.126.070501 for the detail of numerical calculation and additional experimental results.
[28] N. Watanabe and M. Tsukada, Fast and stable method for simulating quantum electron dynamics, Phys. Rev. E **62**, 2914 (2000).
[29] N. E. Fletcher, J. Ebbecke, T. J. B. M. Janssen, F. J. Ahlers, M. Pepper, H. E. Beere, and D. A. Ritchie, Quantized acoustoelectric current transport through a static quantum dot using a surface acoustic wave, Phys. Rev. B **68**, 245310 (2003).
[30] G. R. Aĭzin, Godfrey Gumbs, and M. Pepper, Screening of the surface-acoustic-wave potential by a metal gate and the quantization of the acoustoelectric current in a narrow channel, Phys. Rev. B **58**, 10589 (1998).
[31] S. Rahman, M. Kataoka, C. H. W. Barnes, and H. P. Langtangen, Numerical investigation of a piezoelectric surface acoustic wave interaction with a one-dimensional channel, Phys. Rev. B **74**, 035308 (2006).
[32] R. Takasu, Y. Sato, T. Hata, T. Akiho, K. Muraki, and T. Fujisawa, Surface-acoustic-wave resonators with Ti, Cr, and Au metallization on GaAs, Appl. Phys. Express **12**, 055001 (2019).
[33] J. You, H.-O. Li, K. Wang, G. Cao, X.-X. Song, M. Xiao, and G.-P. Guo, Suppression of low-frequency charge noise in gates-defined GaAs quantum dots, Appl. Phys. Lett. **107**, 233104 (2015).
[34] T. Hayashi, T. Fujisawa, H. D. Cheong, Y. H. Jeong, and Y. Hirayama, Coherent Manipulation of Electronic States in a Double Quantum Dot, Phys. Rev. Lett. **91**, 226804 (2003).
[35] M. Thorwart, J. Eckel, and E. R. Mucciolo, Non-Markovian dynamics of double quantum dot charge qubits due to acoustic phonons, Phys. Rev. B **72**, 235320 (2005).
[36] Y. Chung, H. Hou, S.-K. Son, T.-K. Hsiao, A. Nasir, A. Rubino, J. P. Griffiths, I. Farrer, D. A. Ritchie, and C. J. B. Ford, Quantized charge transport driven by a surface acoustic wave in induced unipolar and bipolar junctions, Phys. Rev. B **100**, 245401 (2019).
[37] T.-K. Hsiao, A. Rubino, Y. Chung, S.-K. Son, H. Hou, J. Pedrós, A. Nasir, G. Éthier-Majcher, M. J. Stanley, R. T. Phillips, T. A. Mitchell, J. P. Griffiths, I. Farrer, D. A. Ritchie, and C. J. B. Ford, Single-photon emission from single-electron transport in a SAW-driven lateral light-emitting diode, Nat. Commun. **11**, 917 (2020).